EXPERIMENTAL STUDY ON SEISMIC RETROFIT OF R/C FRAME WITH DAMPING BRACING

Dagen WENG [1]   Hui HE [2]   Xilin LU [3]

[1]*Professor, College of Civil Engineering, Tongji University, Shanghai, China.*
Email: wdg@mail.tongji.edu.cn
[2]*Ph.D. candidate, College of Civil Engineering, Tongji University, Shanghai, China.*
Email: hehui503@163.com.cn
[3] *Professor, College of Civil Engineering, Tongji University, Shanghai, China.*
Email: lxlst@mail.tongji.edu.cn

ABSTRACT :

The experimental study on seismic retrofit of the reinforced concrete (R/C) frame with damper bracings was carried in this paper. Two test models were cast according to one kind of frame in which gravity load carrying beams were arranged in transverse direction of the building and possessed lower lateral strength in longitudinal direction. One of the models called energy dissipation frame was retrofitted with two supplemental viscous damper bracings in each inter-story in longitudinal direction. Both models were arranged on the shaking table and simultaneously excited in longitudinal direction by simulated earthquake motions with different peak ground acceleration (PGA). The test results showed that the ratios of the inter-story damper forces to the inter-story shear forces ranged from 0.20 to 0.70 and the equivalent damping ratios ranged from 0.14 to 0.28 for the energy dissipation frame. The accelerations, inter-story displacements and inter-story shear forces were greatly reduced comparing to the model without damper bracings. Besides, the vibration in resonance was prevented because of the high damping performances of damper bracings. Given the same inter-story displacements, the energy dissipation frame was tested the twice PGA of the frame without damper bracings. It is verified that the seismic performances of this kind of frame can be improved by the damper bracings.

KEYWORDS: Shaking table test, viscous damper, energy dissipation, seismic retrofit

1. INTRODUCTION

China is one of the countries suffering from serious earthquake damages all over the world. In China, there are a great many old R/C frame structures without anti-seismic measures, and the layouts of frames are unidirectional. For example, the floor slabs are pre-cast slabs and the gravity load carrying beams were arranged in transverse direction of the buildings. For these structures, the distributions of vertical reinforcements of the columns are unidirectional, and the longitudinal connections of the buildings are tie beams which do not carry gravity load, so the longitudinal seismic abilities of the structures are much worse than the transverse seismic abilities. As the seismic abilities of the longitudinal tie beams are poor, these structures can be regarded as strong column-weak beam structures. For these structures, the traditional seismic retrofit methods can be listed as follow:

1)   Enlarging the cross-sections of almost all columns and longitudinal tie beams, 2) Adding shear walls in the longitudinal direction of the old structures and choosing appropriate stiffness and strength of shear walls, so the shear walls can bear 70-80% of the longitudinal earthquake actions.

It is effective to enhance the anti-seismic abilities and the anti-collapse capabilities of the structures through these measures, but if the architectural styles and layouts of some old structures should be maintained, then these measures are unacceptable. For these methods, another problem is that structures could not be in use during retrofitting. Then, the more effective energy dissipation devices are introduced in the seismic retrofit. The measures are to enhance the damping performances of the structures, i.e. its displacements and inelastic deformations to be reduced, so as not to be collapsed under major earthquake. The energy dissipation devices have been widely used for engineering application all over the world. However, there are also some problems

should be solved and verified by tests. For the R/C frame structures added dampers, what are the changes of the dynamic characteristics? How will the energy dissipation capabilities of the structures be enhanced, when the main structure enters elastoplastic state?

2. TEST DESIGN

In the test, two models were arranged on the shaking table and simultaneously excited, in order to decrease the experimental errors caused by different ground excitations. One model was the structure with dampers (model MA), the other model was the structure without dampers (model MB). The dimensions and the excitations of both models were same, in order to measure the vibration reduction effects of dampers. In the test, the non-linear viscous dampers were the main energy dissipation devices and they were braced with steel frames. The ground motions were input along the weak direction of the structures. For each model, the floor height was 1.1m, the total height was 4.4m (the heights of footing beams not to be included), and the total weight was 22 ton(two models). Fig.1 showed an overall view of the both models. The structural properties of the models were shown in the Table 1.

Table 1 Structural properties of the models

Elements & Material	Cross section (width×height) (mm×mm)	Longitudinal steel bar	Stirrup	de (mm)
Columns	90×100 (width along vibration direction was 90)	$6-d8$	$d4@40$(ends of column) $d4@70$ (other positions)	
Frame beams	80×80 (tie beams along vibration direction)	$4-d6$	$d4@70$	10
	80×180 (other beams)	$4-d10$	$d6@40$(ends of beams) $d6@70$ (other positions)	
Footing beams	250×300	$4-d20$	$d8@150$	
Additional mass blocks	Pre-cast slabs, thickness was 70mm, additional weight of each floor was 25kN.			
concretes	For footing beams, normal concrete, C30. For frames, fine concrete,C20 (20MPa).			

Where, dc= thickness of concrete cover measured from the extreme tension fiber to the center of the bar located closest thereto (mm). The time scale was 1.
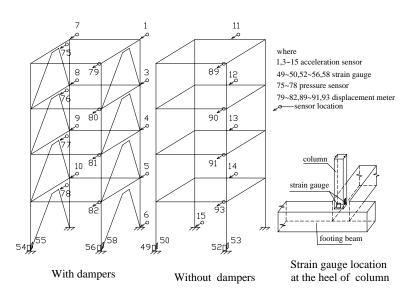

Fig.1 Overall view of the test models

where
1,3~15 acceleration sensor
49~50,52~56,58 strain gauge
75~78 pressure sensor
79~82,89~91,93 displacement meter
○—sensor location

With dampers   Without dampers

Strain gauge location at the heel of column

Fig.2 Sensors location

Table 2   Input motions of the shaking table test

	Input motion	Input peak accel. (g)	Measured peak accel (g)
Wn-1	White noise	0.05 (MA,MB)	
El-2	El Centro	0.05 (MA,MB)	0.051
Sh-3	Shanghai artificial wave	0.05 (MA,MB)	0.060
El-4	El Centro	0.08 (MA,MB)	0.087
Sh-5	Shanghai artificial wave	0.08 (MA,MB)	0.101
El-6	El Centro	0.12 (MA,MB)	0.130
Sh-7	Shanghai artificial wave	0.12 (MA,MB)	0.129
El-8	El Centro	0.15 (MA,MB)	0.160
Sh-9	Shanghai artificial wave	0.15 (MA,MB)	0.155
El-10	El Centro	0.20 (MA,MB)	0.214
Sh-11	Shanghai artificial wave	0.20 (MA,MB)	0.214
Wn-12	White noise	0.05 (MA,MB)	
Wn-13	White noise	0.05 (MA)	
El-14	El Centro	0.25 (MA)	0.256
Sh-15	Shanghai artificial wave	0.25 (MA)	0.297
El-16	El Centro	0.40 (MA)	0.374
Sh-17	Shanghai artificial wave	0.40 (MA)	0.394
Wn-18	White noise	0.05 (MA)	

Where, El represented the El Centro wave (1940, NS), Sh represented the Shanghai artificial wave, Wn represented the white noise.

In the test, the dampers were produced by Shanghai Research Institute of Materials, and the damper force was presented as:

$$F_d = 0.6 \, \text{sgn}(\dot{x}) |\dot{x}|^\alpha \tag{2.1}$$

Where, C_d was the damper coefficient, $\dot{x}$ was the relative velocity of the damper, α was the performance parameter (ranged from 0.1 to 2.0). In the test, $C_d = 0.6 kN/(mm/s)^\alpha$, $\alpha = 0.2$, maximum damper forces ranged from $1.3kN$ to $2.0kN$, maximum displacement was $\pm 45mm$ (measured maximum displacement reached to 60mm). The model design can be referenced from [1].

3. TEST ANALYSIS

3.1. Acceleration Responses Analysis

Fig.3 and Fig.4 showed the measured acceleration curves of the 4-story models under the input motions (El-6, Sh-7). Fig.5 and Fig.6 showed the acceleration response spectra at the 4th floor (curves of other floors were similar). From these figures, it could be found that the responses of model MA were much less than those of model MB. Table 3 showed the peak accelerations and the weighted averages of the acceleration response spectra of models MA and MB. And Table 4 showed the corresponding statistics.

From the figures and data in this part, it could be found that the acceleration responses of model MA at every floor were effectively reduced by the energy dissipation bracings. For the model MA, Table 3 showed that the mean values of $|A_{1i}|/|A_{10}|$ ranged from 0.78 to 1.18, and the corresponding standard deviation ranged from 0.08 to 0.20. For the model MB, Table 3 showed that the mean values of $|A_{0i}|/|A_{00}|$ ranged from 1.38 to 1.84, and the corresponding standard deviation ranged from 0.30 to 0.48. The mean values of $|A_{1i}|/|A_{0i}|$ ranged from 0.60 to 0.69, and the corresponding standard deviation ranged from 0.13 to 0.16. Besides, the mean values of AF_{1i}/AF_{0i} ranged from 0.48 to 0.71, and the corresponding standard deviation ranged from 0.10 to 0.16. In a

word, for the model with dampers, the reductions of the earthquake responses ranged from 30% to 40%.

Table 3 Comparisons of the peak response accelerations

Story NO.	Input motion (g)	MA $\frac{\lvert A_{1i}\rvert}{\lvert A_{10}\rvert}$	MB $\frac{\lvert A_{0i}\rvert}{\lvert A_{00}\rvert}$	$\frac{MA}{MB}$ $\frac{\lvert A_{1i}\rvert}{\lvert A_{0i}\rvert}$	MA $\frac{AF_{1i}}{AF_{10}}$	MB $\frac{AF_{0i}}{AF_{00}}$	$\frac{MA}{MB}$ $\frac{AF_{1i}}{AF_{0i}}$	Input motion (g)	MA $\frac{\lvert A_{1i}\rvert}{\lvert A_{10}\rvert}$	MB $\frac{\lvert A_{0i}\rvert}{\lvert A_{00}\rvert}$	$\frac{MA}{MB}$ $\frac{\lvert A_{1i}\rvert}{\lvert A_{0i}\rvert}$	MA $\frac{AF_{1i}}{AF_{10}}$	MB $\frac{AF_{0i}}{AF_{00}}$	$\frac{MA}{MB}$ $\frac{AF_{1i}}{AF_{0i}}$
4	El-2 (-0.042~0.051)	1.27	1.55	0.82	1.24	2.61	0.47	Sh-9 (-0.155~0.124)	1.33	2.02	0.66	1.52	3.10	0.49
3		1.14	1.24	0.92	1.17	1.97	0.60		0.89	1.52	0.58	1.34	2.34	0.57
2		1.18	1.43	0.82	1.12	1.75	0.64		0.81	1.84	0.44	1.18	2.18	0.54
1		1.02	1.24	0.83	1.04	1.32	0.79		0.81	1.74	0.46	1.04	1.53	0.68
4	Sh-3 (-0.060~0.056)	1.19	3.08	0.39	1.29	4.78	0.27	El-10 (-0.149~0.214)	0.97	1.73	0.56	1.22	1.99	0.61
3		1.08	2.41	0.45	1.27	3.83	0.33		0.62	0.93	0.66	1.08	1.24	0.87
2		0.97	2.17	0.45	1.18	3.06	0.39		0.68	1.23	0.55	0.99	1.44	0.68
1		0.90	1.95	0.46	1.06	1.87	0.57		0.78	1.23	0.63	0.94	1.22	0.77
4	El-4 (-0.062~0.087)	1.30	1.47	0.88	1.24	3.00	0.41	Sh-11 (-0.214~0.158)	1.29	1.53	0.84	1.61	1.99	0.73
3		0.99	1.10	0.89	1.17	2.33	0.50		0.86	1.07	0.80	1.36	1.24	0.85
2		0.92	1.15	0.79	1.10	2.09	0.53		0.79	1.21	0.65	1.16	1.44	0.74
1		0.83	1.03	0.80	1.03	1.48	0.69		0.78	1.23	0.63	1.03	1.22	0.84
4	Sh-5 (-0.101~0.082)	1.26	2.08	0.6	1.39	2.73	0.51	El-14 (-0.166~0.254)	0.82			1.20		
3		0.98	1.65	0.59	1.32	2.12	0.62		0.56			0.98		
2		0.83	1.44	0.58	1.18	1.79	0.66		0.63			0.90		
1		0.85	1.7	0.5	1.06	1.34	0.79		0.74			0.92		
4	El-6 (-0.092~0.130)	1.15	1.51	0.77	1.23	2.65	0.38	Sh-15 (-0.297~0.258)	1.45			1.62		
3		0.80	1.37	0.58	1.15	2.23	0.45		0.87			1.20		
2		0.76	1.37	0.56	1.06	2.22	0.45		0.73			1.02		
1		0.76	1.22	0.62	0.98	1.69	0.59		0.76			0.97		
4	Sh-7 (-0.092~0.130)	1.29	1.84	0.70	1.45	2.74	0.53	El-16 (-0.283~0.374)	0.90			0.99		
3		0.94	1.26	0.75	1.33	2.12	0.63		0.49			0.82		
2		0.81	1.26	0.64	1.18	1.86	0.64		0.51			0.80		
1		0.81	1.47	0.56	1.05	1.38	0.76		0.93			0.93		
4	El-8 (-0.115~0.160)	1.03	1.63	0.63	1.21	3.26	0.37	Sh-17 (-0.394~0.348)	1.22			1.25		
3		0.68	1.23	0.55	1.11	2.47	0.45		0.70			0.96		
2		0.67	1.38	0.49	1.02	2.35	0.43		0.58			0.89		
1		0.77	1.26	0.61	0.96	1.65	0.58		0.74			0.92		

Where, $\lvert A_{1i}\rvert$, $\lvert A_{0i}\rvert$ - absolute peak accelerations at the ith floor of the models MA and MB, respectively.

$\lvert A_{10}\rvert$, $\lvert A_{00}\rvert$ - absolute peak accelerations at the footing beams of the models MA and MB, respectively.

AF_{1i}, AF_{0i} - weighted averages of the acceleration response spectra at the ith floor of the models MA and MB, respectively (i.e. that is equal to the area which is enclosed by the acceleration spectra coordinates and periods from 0.1~0.4s over 3.99s).
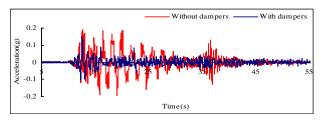
AF_{10}, AF_{00} - weighted averages of the acceleration response spectra at the footing beam of the models MA and MB, respectively.

Table 4 Statistics of the peak response accelerations

Story No.	MA $\frac{\lvert A_{1i}\rvert}{\lvert A_{10}\rvert}$		MB $\frac{\lvert A_{0i}\rvert}{\lvert A_{00}\rvert}$		MA/MB $\frac{\lvert A_{1i}\rvert}{\lvert A_{0i}\rvert}$		MA $\frac{\lvert A_{1i}\rvert}{\lvert A_{0i}\rvert}$		MB $\frac{AF_{0i}}{AF_{00}}$		MA/MB $\frac{AF_{1i}}{AF_{0i}}$	
	μ	σ	μ	σ	μ	σ	μ	σ	μ	σ	μ	σ
4	1.18	0.18	1.84	0.48	0.69	0.15	1.32	0.17	2.89	0.75	0.48	0.12
3	0.83	0.20	1.38	0.42	0.68	0.16	1.16	0.16	2.19	0.68	0.59	0.16
2	0.78	0.17	1.45	0.32	0.60	0.13	1.06	0.12	2.02	0.46	0.57	0.11
1	0.82	0.08	1.41	0.30	0.61	0.13	1.00	0.05	1.47	0.2	0.71	0.09

Where, μ - mean value of the peak response accelerations, σ - standard deviation.
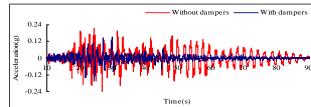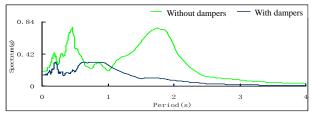
Fig.3. Acceleration response, 4th floor, input El-6

Fig.4. Acceleration response, 4th floor, input Sh-7
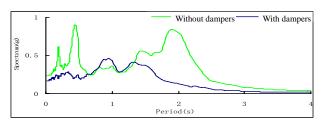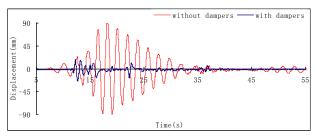

Fig.5. Acceleration response spectra, 4th floor, input El-6

Fig.6. Acceleration response spectra, 4th floor, input Sh-7

3.2. Displacement Responses Analysis

Fig.7 and Fig.8 showed the measured curves of the inter-story displacement response at the 4th floor under the input motions El-6, Sh-7, respectively. Table 5 showed the peak displacements of models MA and MB under different input motions, and Table 6 showed the corresponding statistics of the models MA and MB.
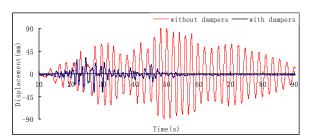

Fig.7 Displacement response, 4th floor, input El-6

Fig.8 Displacement response, 4th floor, input Sh-7

Table 5   Comparison of the peak inter-story displacements

Story No.	Input motion	MA θ_{1i}	MB θ_{0i}	$\dfrac{MA}{MB}$ $\dfrac{\theta_{1i}}{\theta_{0i}}$	Input motion	MA θ_{1i}	MB θ_{0i}	$\dfrac{MA}{MB}$ $\dfrac{\theta_{1i}}{\theta_{0i}}$	Input motion	MA θ_{1i}	MB θ_{0i}	$\dfrac{MA}{MB}$ $\dfrac{\theta_{1i}}{\theta_{0i}}$	Input motion	MA θ_{1i}	MB θ_{0i}	$\dfrac{MA}{MB}$ $\dfrac{\theta_{1i}}{\theta_{0i}}$
4	El-2	1/1192	1/80	0.07	El-6	1/299	1/28	0.09	El-10	1/168	1/40	0.24	El-16	1/49		
3		1/583	1/114	0.20		1/190	1/41	0.22		1/102	1/21	0.21		1/40		
2		1/337	1/61	0.18		1/140	1/19	0.14		1/81	1/25	0.31		1/38		
1		1/488	1/193	0.40		1/186	1/64	0.34		1/117	1/62	0.53		1/74		
4	Sh-3	1/716	1/30	0.04	Sh-7	1/199	1/28	0.14	Sh-11	1/76	1/21	0.28	Sh-17	1/25		
3		1/321	1/44	0.14		1/113	1/31	0.27		1/49	1/16	0.33		1/20		
2		1/217	1/21	0.10		1/88	1/19	0.22		1/45	1/12	0.27		1/20		
1		1/228	1/67	0.29		1/129	1/71	0.55		1/70	1/37	0.53		1/40		
4	El-4	1/627	1/43	0.07	El-8	1/234	1/24	0.10	El-14	1/102						
3		1/271	1/62	0.23		1/147	1/29	0.20		1/72						
2		1/196	1/29	0.15		1/117	1/16	0.14		1/64						
1		1/304	1/102	0.34		1/153	1/56	0.37		1/115						
4	Sh-5	1/295	1/34	0.12	Sh-9	1/138	1/21	0.15	Sh-15	1/37						
3		1/157	1/37	0.24		1/80	1/22	0.28		1/27						
2		1/116	1/24	0.21		1/67	1/14	0.21		1/24						
1		1/162	1/87	0.54		1/106	1/43	0.41		1/47						

Where, θ_{1i}, θ_{0i} was the inter-story drift angle at the ith floor of the model MA and model MB, respectively.

From the tables and figures in this part, it could be found as follow:

1) The inter-story displacements of model MA were much smaller than those of model MB. Table 6 showed that the mean values of the inter-story drift angle ratios (θ_{1i}/θ_{0i}) ranged from 0.13 to 0.43, the corresponding standard deviation ranged from 0.06 to 0.10.

2) The last input motion was the Shanghai artificial wave. For the model MB, when the PGA was 200gal (cm/s^2), cracks appeared at the nodes of the 2nd, 3rd, and 4th floor and a severe damage behavior appeared. However, for the model MA, the PGA was up to 400gal and the corresponding cracks appeared at some nodes of 2nd, 3rd floor and a moderate or more damage behavior appeared only.

3) The model MA was stronger than model MB. For example, when the inter-story drift angles of models MA and MB reached to the same value 1/20, the measured corresponding input peak accelerations should be 0.394g and 0.129g, respectively. The ratio of PGA of MA to that of MB could be 3. That is to say, the seismic bearing capacity of MA structure was enhanced by twice comparing to the model MB.

Table 6   Statistics of peak displacement

Story No.	1th		2nd		3rd		4th	
	μ	σ	μ	σ	μ	σ	μ	σ
θ_{1i}/θ_{0i}	0.13	0.08	0.22	0.06	0.19	0.06	0.43	0.10

3.3. Analysis of the Energy Dissipation Performances of the Dampers and the Inter-story Shear Forces

Fig. 9 and Fig. 10 showed the measured inter-story displacement and damper force relationship curves at the 2nd floor，where the corresponding inputs being El-6 and Sh-7, respectively (curves of other stories were similar). Table 7 and Table 8 showed the maximum inter-story shear forces, the maximum damper forces, the ratios of the inter-story damper forces to inter-story shear forces, and the equivalent damping ratios.
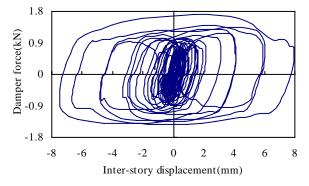

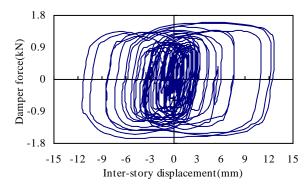Fig.9 Inter-story displacement and damper force relationship curves, 2nd floor, input El-6

Fig.10 Inter-story displacement and damper force relationship curves, 2nd floor, input Sh-7.

Table 7   Comparison of peak inter-story shear forces

Story No.	Input motion	MA Q_{1i}	MB Q_{0i}	$\frac{MA}{MB}$ $\frac{Q_{1i}}{Q_{0i}}$	Input motion	MA Q_{1i}	MB Q_{0i}	$\frac{MA}{MB}$ $\frac{Q_{1i}}{Q_{0i}}$	Input motion	MA Q_{1i}	MB Q_{0i}	$\frac{MA}{MB}$ $\frac{Q_{1i}}{Q_{0i}}$	Input motion	MA Q_{1i}	MB Q_{0i}	$\frac{MA}{MB}$ $\frac{Q_{1i}}{Q_{0i}}$
4	El-2	1.63	1.98	0.82	El-6	3.75	4.89	0.77	El-10	5.20	9.26	0.56	El-16	8.39		
3		3.06	3.38	0.91		4.63	7.47	0.62		6.08	6.78	0.90		9.23		
2		4.55	5.21	0.87		5.37	9.56	0.56		8.05	7.07	1.14		10.49		
1		3.93	4.38	0.90		7.43	11.19	0.66		10.09	10.79	0.94		11.36		

4		1.88	4.86	0.39		4.17	5.93	0.70		6.90	8.17	0.84		12.04
3	Sh-3	3.51	7.99	0.44	Sh-7	6.65	7.58	0.88	Sh-11	10.97	9.62	1.14	Sh-17	17.39
2		4.79	9.98	0.48		8.17	8.84	0.92		12.05	12.66	0.95		16.68
1		5.64	10.95	0.52		9.06	10.75	0.84		13.92	15.61	0.89		16.23
4		2.82	3.20	0.88		4.10	6.51	0.63		5.22				
3	El-4	3.94	4.93	0.80	El-8	4.95	8.67	0.57	El-14	7.73				
2		4.43	5.78	0.77		6.39	10.57	0.60		9.00				
1		4.91	6.60	0.74		8.68	12.54	0.69		8.96				
4		3.19	5.24	0.61		5.16	7.82	0.66		10.80				
3	Sh-5	5.45	6.41	0.85	Sh-9	8.13	9.01	0.90	Sh-15	14.66				
2		6.91	7.31	0.95		9.54	11.87	0.80		16.33				
1		7.96	9.03	0.88		10.77	14.99	0.72		17.19				

Table 8   Maximum average damper forces and damping ratios

Story No.	Input motion	DF_{ij}	$\frac{2\left\|DF_{ij}\right\|_{max}}{Q_{i\,max}}$	W_{si}	W_{ci}	ζ_a	Input motion	DF_{ij}	$\frac{2\left\|DF_{ij}\right\|_{max}}{Q_{i\,max}}$	W_{si}	W_{ci}	ζ_a
4		0.93	1.14	0.75	5.49			1.55	0.60	20.57	79.07	
3	El-2	0.82	0.54	2.89	9.90	0.35	Sh-9	1.29	0.32	55.89	113.52	0.20
2		1.19	0.52	7.43	24.86			1.77	0.37	78.31	185.98	
1		1.03	0.52	4.43	14.86			1.45	0.27	55.88	96.30	
4		1.01	1.07	1.44	9.93			1.6	0.62	17.02	67.05	
3	Sh-3	0.86	0.49	6.01	18.86	0.31	El-10	1.33	0.44	32.78	91.80	0.23
2		1.23	0.51	12.14	39.90			1.78	0.44	54.66	154.71	
1		1.09	0.39	13.61	33.66			1.46	0.29	47.43	87.85	
4		1.17	0.83	2.47	13.14			1.82	0.53	49.93	168.59	
3	El-4	0.99	0.50	8.00	25.72	0.31	Sh-11	1.47	0.27	123.13	211.20	0.17
2		1.4	0.63	12.43	50.29			1.93	0.32	147.28	301.94	
1		1.21	0.49	8.88	28.02			1.6	0.23	109.37	160.91	
4		1.31	0.82	5.95	31.26			1.71	0.66	28.15	118.02	
3	Sh-5	1.08	0.40	19.09	48.43	0.25	El-14	1.43	0.37	59.05	139.82	0.23
2		1.51	0.44	32.76	91.64			1.9	0.42	77.34	209.00	
1		1.29	0.32	27.02	56.06			1.59	0.35	42.85	97.34	
4		1.33	0.71	6.90	31.32			2.2	0.41	160.54	418.59	
3	El-6	1.12	0.48	13.40	41.50	0.27	Sh-15	1.71	0.23	298.63	445.87	0.14
2		1.57	0.58	21.10	78.95			2.23	0.27	374.23	654.13	
1		1.33	0.36	21.97	50.34			1.83	0.21	201.16	274.11	
4		1.39	0.67	11.53	49.17			1.94	0.46	94.17	278.73	
3	Sh-7	1.19	0.36	32.37	74.14	0.22	El-16	1.63	0.35	126.91	286.88	0.19
2		1.64	0.40	51.06	131.20			2.03	0.39	151.83	376.08	
1		1.38	0.30	38.63	75.31			1.69	0.30	84.43	160.78	
4		1.42	0.69	9.64	42.72			2.39	0.40	264.88	673.02	
3	El-8	1.2	0.48	18.52	57.47	0.26	Sh-17	1.81	0.21	478.23	637.12	0.14
2		1.65	0.52	30.04	99.28			2.28	0.27	458.70	802.56	
1		1.37	0.32	31.20	63.04			1.9	0.23	223.16	334.40	

Where, DF_{ij} represented the measured peak absolute value of the damper force of the jth damper at the ith floor of model MA, and in the test, it was represented by the average between positive peak damper force and negative peak damper force. $Q_{i\,max}$ represented the peak inter-story shear force at the ith floor of model MA. It can be calculated as follow:

$$Q_{i\,max} = Max\left|\sum_{i=i}^{4} A_i(t)M_i\right| \tag{3.1}$$

In which, M_i is the mass of the ith floor, $A_i(t)$ is the acceleration at the ith floor.

According to Chinese Code for Seismic Design of Buildings [2], the total damping ratio of the structure with

energy dissipation devices can be calculated as follow:

$$\zeta = \zeta_s + \zeta_a \qquad (3.2)$$

Where, ζ_s is the damping ratio of the structure without energy dissipation devices, ζ_a is the additional damping ratio of the structure with energy dissipation devices and ζ_a is given by:

$$\zeta_a = \frac{W_c}{4\pi W_s} \qquad (3.3)$$

In which, W_s is the associated maximum strain energy:

$$W_s = \frac{1}{2}\sum_{i=1}^{4}[M_i \times \frac{(A_{1i}+|A_{-1i}|)}{2} \times \frac{(D_{1i}+|D_{-1i}|)}{2}] \qquad (3.4)$$

Where, A_{1i}、A_{-1i} - the positive and negative peak accelerations of MA at ith floor，respectively. D_{1i}、D_{-1i} - the positive and negative peak displacements of MA at ith floor relative to footing beam, respectively. While W_c is the energy dissipated by the energy dissipation system in a single cycle of motion at the maximum expected displacement:

$$W_c = \sum_{i=1}^{4}W_{ci} = \sum_{i=1}^{4}\sum_{j=1}^{2}(|DF_{ij}|_{max}) \times \beta_{ij} \times [\frac{(D_{1i}+|D_{-1i}|)}{2} - \frac{|DF_{ij}|_{max}}{K^*_{b(ij)}}] \times 4 \qquad (3.5)$$

Where, β_{ij} - a reduction coefficient (approximately ranges from 0.80 to 1.0) of the jth damper at the ith floor, which is the ratio of the area of measured hysteretic loop to area of an ideal parallelogram. In this paper, it is 0.7~0.9.

$$|DF_{ij}|_{max} = (DF_{ij} + |DF_{-ij}|)/2 \qquad (3.6)$$

Where, DF_{ij}、DF_{-ij} - the positive or negative peak damper force of the jth damper at the ith floor，respectively.
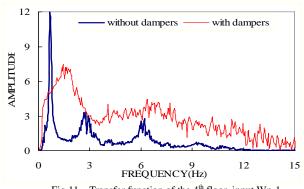
According to the maximum inter-story damper forces and the inter-story shear forces shown in the Table 7 and Table 8, the equivalent damping ratios under varied input motions could be obtained and they were shown in the Table 8. From the energy dissipation performance curves of the dampers and the data in the tables, some conclusions could be drawn as follow:
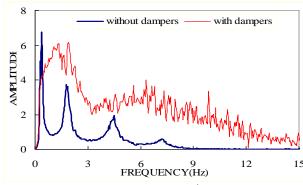
1) From the comparisons of the inter-story shear forces of the two models, it could be found that the inter-story shear forces of model MB were larger than those of model MA. However, for the inter-story shear forces at the 2nd floor (under input El-10) and the 3rd floor (under input Sh-11), they were not. The reason was that under these two input motions, both models cracked seriously, the natural frequencies decreased, and the earthquake actions declined. The ratios of inter-story shear forces of the model MA to that of MB ranged from 0.39 to 0.92.That is to say, for the model with dampers, the reductions of the inter-story shear forces ranged from 8% to 61%.

2) For the model MA, under the strong input motions (El-14, El-16, Sh-15, Sh-17), the maximum inter-story shear forces at different floors were almost the same. Besides, the shear strengths of the lower floors were enhanced, so the overall seismic performances of the structure were improved. The shapes of the damper force and inter-story displacement relation hysteretic curves were parallelogram, which showed good energy dissipation performances. Under all input motions, the damper forces varied from 0.8 kN to 2.3 kN, which were expected.

3) For the model MA, the ratios of the inter-story damper forces to the inter-story shear forces ranged from 0.20 to 0.70 (excepting the ratios of the 4th floor under inputs El-2 and Sh-3). The average equivalent damping ratios ranged from 0.14 to 0.28. And the equivalent damping ratios were different under different input motions. If the excitations were stronger, the calculated equivalent damping ratios would be smaller. The reason was the nonlinear properties of dampers. In the test, the measured data showed that the damper forces and equivalent damping ratios were appropriate.

3.4. Dynamic Characteristics Analysis

For the input motions Wn-1, Wn-12, Wn-13, and Wn-18 in the Table 2, the PGA was 0.05g. The small amplitude excitations were introduced to learn on the stiffness degradation of the structure. Fig.11 and Fig.12 showed the transfer functions of relative accelerations (in the Fig.11 and Fig.12, the amplitudes of model MA were amplified by 4 times to make the curves more distinct). From the Fig.11 and Fig.12, it could be figured out as follow:

Fig.11   Transfer function of the 4th floor, input Wn-1

Fig.   12 Transfer function of the 4th floor, input Wn-12

Table 9   Dynamic characteristics of the structures under white noise (frequencies and modes)

Story No.	Model MB						Model MA			
	Wn-1			Wn-12			Wn-1	Wn-12	Wn-13	Wn-18
	1st mode (0.68Hz)	2nd mode (2.64Hz)	3rd mode (6.2Hz)	1st mode (0.39Hz)	2nd mode (1.86Hz)	3rd mode (4.49Hz)	1st mode (1.46Hz)	1st mode (1.37z)	1st mode (1.03Hz)	1st mode (1.03Hz)
4	1.00	0.87	0.58	1.00	0.89	0.50	1.00	1.00	1.00	1.00
3	0.84	0.23	-0.83	0.85	-0.32	-0.89	0.88	0.97	0.95	0.94
2	0.60	-1.00	0.07	0.65	-1.00	0.19	0.82	0.89	0.89	0.87
1	0.27	-0.69	1.00	0.25	-0.59	1.00	0.65	0.73	0.76	0.76

1) For the transfer functions of model MA, there was only one predominant peak and the shape of the amplitudes would not change under different damage states. By contrast, for the transfer functions of model MB, there were many predominant peaks and the positions of these peaks changed as the damage states changed. Judging from the amplitude spectra and the phase spectra, the first mode of MA could be obtained just only, and the reason was the high damping properties of the structure. However, for the model MB, the first three modes could be obtained.

2) For the model MA, the curves of the peak points were relatively flat, reflecting the high damping performances. However, for the model MB, the peak amplitudes of transfer functions were larger than those of model MA, the structure was more likely to vibrate in resonance at the peak points, and the reason was the low damping performances of the structure. From the displacement time history curves and the acceleration time history curves, it could be found that the peak values were decreased.

3) From Table 9, it could be found that under four different input motions, the fundamental frequencies of the model MA almost did not change with the help of the damper bracings. The deformations were small, and the ratios of the fundamental frequencies of model MA to those of model MB ranged from 2.15 to 3.51. Generally speaking, the inter-story shear forces of the model MB should be larger than those of the model MA. But in fact, the results in the test were contrast to the original expectation. The reason was that the initial stiffness of the damper bracing was large, which was related to the nonlinear characteristics of the dampers.

In a word, the energy dissipation bracings provided effective high damping performances and avoided vibrating in resonance.

3.5. Inter-story Displacement Time History and Damper Force Time History

Fig.13 showed the time history of inter-story displacement and damper force. It could be found that the phase differences between the maximum inter-story displacements and the maximum damper forces were not the ideal value 90°. And the phase differences were influenced by the bracing stiffness and the initial stiffness of the dampers. The design forces of the components which are connected to the dampers should be the maximum of the sum of the forces of the components by inter-story displacement and the damper forces. And for these components, the damper forces were the large additional forces.
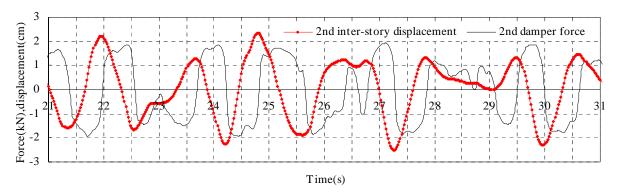

Fig.13   Comparisons of the time history of inter-story displacement and the damper force of 2nd floor, input Sh-11

4. CONCLUSIONS

As an effective way in the seismic retrofit, the efficiencies of damper bracings were verified by test. In the test, it was found that if the damper bracings were appropriately designed, the earthquake actions could be reduced, the deformations could be decreased and the anti-seismic abilities could be effectively enhanced. For the structures without any anti-seismic measures, damper bracings are very useful and effective measures to mitigate the seismic damages.

REFERENCES

1. WENG Da-gen, LU xi-lin.(2004). Study on design parameters of energy dissipation structures with experiment verification. *Earthquake Engineering and Engineering Vibration* **24:2,** 150-157.
2. China Ministry of Construction.(2001).Code for seismic design of buildings(GB50011-2001).*China Architecture & Building Press*.